Discharging dynamics in an electrolytic cell

Sarah E. Feicht, Alexandra E. Frankel, and Aditya S. Khair[*]

Department of Chemical Engineering, Carnegie Mellon University, Pittsburgh, Pennsylvania 15213, USA

We analyze the dynamics of a discharging electrolytic cell comprised of a binary symmetric electrolyte between two planar, parallel blocking electrodes. When a voltage is initially applied, ions in the electrolyte migrate towards the electrodes, forming electrical double layers. After the system reaches steady state and the external current decays to zero, the applied voltage is switched off and the cell discharges, with the ions eventually returning to a uniform spatial concentration. At voltages on the order of the thermal voltage $V_T = k_B T/q \simeq 25$ mV, where k_B is Boltzmann's constant, T is temperature, and q is the charge of a proton, experiments on surfactant-doped nonpolar fluids observe that the temporal evolution of the external current during charging and discharging is not symmetric [V. Novotny and M. A. Hopper, J. Electrochem. Soc. **126**, 925 (1979); P. Kornilovitch and Y. Jeon, J. Appl. Phys. **109**, 064509 (2011)]. In fact, at sufficiently large voltages (several V_T), the current during discharging is no longer monotonic: it displays a "reverse peak" before decaying in magnitude to zero. We analyze the dynamics of discharging by solving the Poisson-Nernst-Planck equations governing ion transport via asymptotic and numerical techniques in three regimes. First, in the "linear regime" when the applied voltage V is formally much less than V_T, the charging and discharging currents are antisymmetric in time; however, the potential and charge density profiles during charging and discharging are asymmetric. The current evolution is on the RC timescale of the cell, $\lambda_D L/D$, where L is the width of the cell, D is the diffusivity of ions, and λ_D is the Debye length. Second, in the (experimentally relevant) thin-double-layer limit $\epsilon = \lambda_D/L \ll 1$, there is a "weakly nonlinear" regime defined by $V_T \lesssim V \lesssim V_T \ln(1/\epsilon)$, where the bulk salt concentration is uniform; thus the RC timescale of the evolution of the current magnitude persists. However, nonlinear, voltage-dependent, capacitance of the double layer is responsible for a break in temporal antisymmetry of the charging and discharging currents. Third, the reverse peak in the discharging current develops in a "strongly nonlinear" regime $V \gtrsim V_T \ln(1/\epsilon)$, driven by neutral salt adsorption into the double layers and consequent bulk depletion during charging. The strongly nonlinear regime features current evolution over three timescales. The current decays in magnitude on the double layer relaxation timescale, λ_D^2/D; then grows exponentially in time towards the reverse peak on the diffusion timescale, L^2/D, indicating that the reverse peak is the results of fast diffusion of ions from the double layer layer to the bulk. Following the reverse peak, the current decays exponentially to zero on the RC timescale. Notably, the current at the reverse peak and the time of the reverse peak saturate at large voltages $V \gg V_T \ln(1/\epsilon)$. We provide semi-analytic expressions for the saturated reverse peak time and current, which can be used to infer charge carrier diffusivity and concentration from experiments.

I. INTRODUCTION

Charge carriers accumulate at a charged interface, forming electric double layers comprising a diffuse layer and fixed charge on a surface [1]. Electrical double layers are a key component of electrochemical systems. For example, capacitive desalination exploits double layers adjacent to high surface area electrodes to separate ions from the bulk solution [2–4]. Electrochemical capacitors store charge at the electrode-electrolyte interface for energy storage applications, and are notable for their high power compared to batteries and energy density compared to conventional capacitors [5–8]. A simple device exhibiting charge separation is an electrolytic cell, e.g., parallel plate blocking electrodes that charge and discharge in response to cycling the applied voltage [9]. An applied voltage leads to a separation of ionic charge in solution that generates a non-uniform electric field across the device, with a higher electric field in the double layers and a lower electric field in the electroneutral bulk of the cell. The ions accumulate in double layers adjacent to the electrode surface

that are typically thin compared to the width of the cell. The width of the diffuse double layer is characterized by the Debye length, $\hat{\lambda}_D = \sqrt{\hat{\varepsilon} \hat{k}_B \hat{T}/2\hat{q}^2 \hat{c}_0}$, where $\hat{\varepsilon}$ is the permittivity, $\hat{k}_B$ is Boltzmann's constant, $\hat{T}$ is temperature, $\hat{q}$ is the charge of a proton, and $\hat{c}_0$ is the initial concentration of ions. Variables and parameters with a carat superscript are dimensional, while those without a carat are dimensionless. When the applied voltage is switched off, the cell discharges as the ions eventually return to a uniform concentration distribution. The external current spikes in response to the step changes in voltage, and then eventually decays in magnitude to zero. This spike and decay in the magnitude of the external current is seen during both the charging and discharging process.

One might expect that given the globally cyclic nature of the charging and discharging process, the temporal evolution of the external current during charging would be antisymmetric (i.e., opposite in sign but equal in magnitude) to the current during discharging. However, experiments at high voltages compared to the thermal voltage V_T in nonpolar fluids doped with surfactant [10–13] show that while the current during charging monotonically decays, the discharging current is nonmonotonic, resulting in a maximum and minimum in

---
[*]Corresponding author: akhair@andrew.cmu.edu

the current. The maximum in the magnitude of the current is referred to as the "reverse peak" [13]. Nonpolar fluids are doped with surfactant that self-assemble into inverse micelles to stabilize charges, thereby preventing undesirable buildup of large electric potentials [14], in systems ranging from petroleum [15,16] to electronic inks [10,17]. Novotny and Hopper [12] reported a reverse peak in the external current while measuring the current response to a field applied to xylene doped with Aerosol OT. They suggest that the non-monotonic current response stems from dissociation and recombination of the charge carriers, in this case surfactant micelles. Novotny [11] performed similar experiments for blocking and nonblocking electrodes, and compared to numerical solutions of the Poisson-Nernst-Planck (PNP) equations describing the diffusion and migration of charge carriers in a fluid. Novotny included a term for bulk dissociation and recombination of the micellar charge carriers, as well as Faradaic reactions at the electrode interfaces to account for nonblocking electrodes. Novotny found that the blocking electrode model matches experiments when dissociation and recombination are included, to account for charge transfer between micellar charge carriers.

Kornilovitch and Jeon [13] measured the current carried by poly-isobuthylene succinimide inverse micelles in IsoparM during charging and discharging of parallel plate electrodes and also compared the results to the numerical solution of the PNP equations. They did not include a term for dissociation and recombination, yet observed a reverse peak; thus recombination is not necessary to the formation of a reverse peak. Kornilovitch and Jeon [13] proposed a relation between the time the reverse peak occurs $\hat{t}_p$, measured from the time when the voltage is turned off, to the diffusivity of the charge carriers, $\hat{D} \sim 0.1(\hat{L}^2/\hat{t}_p)$, accurate to 50%, where $\hat{L}$ is the width of the device. Their analysis assumes that the charge carriers are monodisperse and have equal diffusivities. This effort to provide an estimate of the charge carrier diffusivity can supplement existing characterization methods for charge transport in doped nonpolar fluids, including measuring conductivity as a function of dopant concentration [18] and performing dynamic light scattering for charge carrier mobility [10]. The transient, frequency-dependent current measured during electrical impedance spectroscopy (subjecting material to small amplitude AC voltage) can also be fit to standard circuit models to calculate the double layer capacitance and Debye length of doped nonpolar fluids [19,20]. Further, in a discharging experiment the total concentration of the charge carriers in the cell can be calculated by integrating the current with respect to time at high voltage [13,21]. The charge carrier mobility can be calculated from the initial current during charging and discharging [21], however this is challenging due to the initial spike in the current.

At high voltages $V \gg V_T$, the dynamics during discharging are fundamentally different from the dynamics during charging [12,13]. Bazant *et al.* [9] performed asymptotic analysis and numerical computations to model the charging dynamics of an electrolytic cell at the experimentally relevant limit of thin Debye lengths, $\hat{\lambda}_D \ll L$. They solved the PNP equations for charge transport in three regimes based on the magnitude of the applied voltage $\hat{V}$ compared to the thermal voltage, $\hat{V}_T = \hat{k}_B\hat{T}/\hat{q}$. The "linear regime" where

the applied voltage is less than the thermal voltage, formally $\hat{V} \ll \hat{V}_T$, is characterized by a uniform bulk salt concentration profile everywhere in the cell, where the salt concentration is equal to the mean of the cation and anion concentration. The double layers behave as linear (voltage-independent) capacitors here, and the charging dynamics is on the *RC* timescale. The "weakly nonlinear" regime occurs at an applied voltage $1 \lesssim \hat{V} < \hat{V}_T \ln 1/\epsilon$. Here, at the limit of thin double layers $\hat{\lambda}_D \ll \hat{L}$, the salt concentration is uniform in the bulk electroneutral electrolyte, but the double layers behave as nonlinear capacitors, meaning that the total charge stored increases nonlinearly with the applied voltage. Again, charging is on the charging *RC* timescale, but now capacitance is a function of voltage. In the "strongly nonlinear" regime, $\hat{V} \gtrsim \hat{V}_T \ln 1/\epsilon$, the bulk is depleted of ions due to neutral salt adsorption by the double layers, where depletion refers to a bulk salt concentration lower than the initial concentration $\hat{c}_0$. In contrast to the linear and weakly nonlinear regimes, here charging occurs on the diffusion timescale. Bazant *et al.* [9] report asymptotic and numerical solutions for the linear and weakly nonlinear regimes, and derive effective macro-scale equations for the strongly nonlinear regime. Beunis *et al.* [22] solved the PNP equations at specific limits of the dynamics of charging, including an extreme case of full charge separation at very large voltage $\hat{V} \gg \hat{V}_T \ln 1/\epsilon$, resulting in transient space charge layers and a power-law decay in the external current. The possibility of a transient space-charge was also suggested by Bazant *et al.* [9].

We adapt the analysis of Bazant *et al.* [9] to solve for the current during discharging in the linear and weakly nonlinear regime. The initial condition for each of these analyses is the steady-state solution derived by Bazant *et al.* [9] after the system has fully charged. In the linear regime, the charging and discharging current are found to be antisymmetric, although the potential and charge density are not. In the weakly nonlinear regime, the magnitude of the discharging current decays to zero over a longer period of time than the charging current, breaking the antisymmetry between current during charging and discharging. However, the current in the weakly nonlinear regime monotonically decays in magnitude, indicating that an analysis of the strongly nonlinear regime, where neutral salt is transferred between the double layer and the bulk, is necessary to capture the reverse peak in the current. At applied voltages several times larger than the thermal voltage during charging, the bulk is depleted of ions due to the large capacitance of the double layers. This bulk depletion and subsequent replenishment during discharging is a characteristic feature of the strongly nonlinear regime that is not included in the weakly nonlinear analysis.

This paper begins with a presentation of the governing Poisson-Nernst-Planck equations and boundary conditions. Numerical calculations used to verify our asymptotic results are presented in Sec. III. In Sec. IV, we solve the linear regime equations via a Laplace transform for small voltages. In Sec. V, we compare the discharging current to the charging current in the weakly nonlinear regime. We present numerical solutions to the PNP equations for the strongly nonlinear regime in Sec. VI and analyze the dynamics of discharging at three relevant timescales. We then provide a discussion on the physics behind the reverse peak. In Sec. VII, we quantify
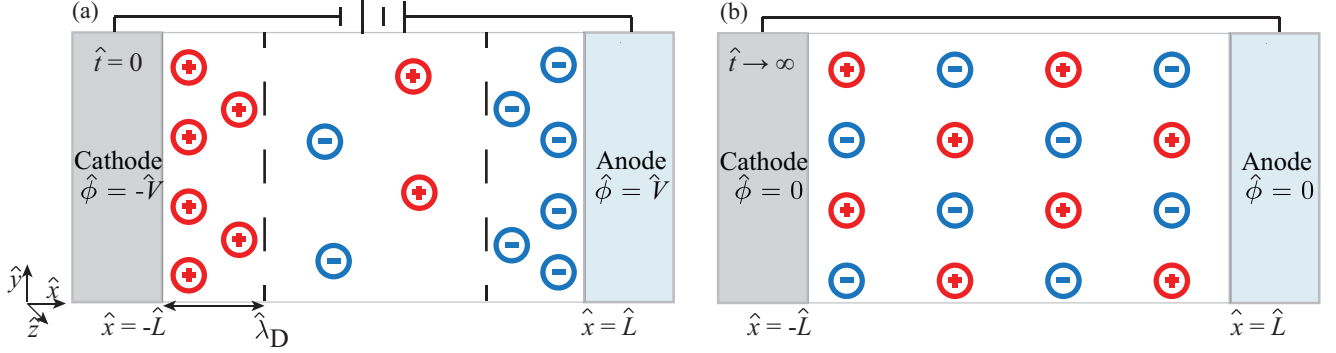
FIG. 1. Schematic of discharging dynamics in an electrolytic cell immediately before discharging (a) and at steady state at long times (b). (a) Initially, at $\hat{t} = 0$ ions are concentrated in double layers at the electrodes and uniformly distributed in the bulk. At $\hat{t} = 0$, the applied field is switched off and (b) the ions eventually redistribute to a uniform concentration profile.

the saturation of the reverse peak at very large voltage and provide semi-analytic expressions for the reverse peak current and time. The charge carrier diffusivity and concentration can be estimated from these expressions. Finally, we conclude in Sec. VIII with a summary of our findings and suggestions for future work.

II. MATHEMATICAL MODEL

We consider a binary, symmetric electrolyte containing ions of equal diffusivity sandwiched between planar, parallel, blocking electrodes. In the absence of an applied field or a charged electrode surface at steady state, the ionic concentration within the electrolyte is uniform. When a potential difference is applied across the electrodes, ions migrate leading to an external current that charges the electrodes. The system reaches steady state when the ion flux decays to zero throughout the cell. This redistribution of ions is reflected in the external current, which spikes when the applied voltage is suddenly switched on then decays to zero at steady state. There are no Faradaic reactions so the ion flux at the electrodes is always zero. We use the variable $\hat{t}$ to denote time during the discharging process, whereas time is denoted as $\hat{s}$ during charging. The applied voltage is switched on at $\hat{s} = 0$ and switched off at $\hat{t} = 0$. Figure 1 depicts the moment when the applied voltage is switched off. The ions initially pinned in the double layer redistribute into the electroneutral bulk, discharging the parallel plate electrodes. As $\hat{t} \to \infty$, the ions return to a uniform concentration profile and the external current again reaches zero. Thus, the system considered here is such that the total number of ions in the cell is conserved throughout time. That is, the electrolytic cell is closed, as opposed to being in contact with a reservoir across which ions could be exchanged during the charging and discharging processes. Our goal is to quantify the external current dynamics during discharging of the electrolytic cell.

We apply the PNP equations to model the discharging dynamics. We neglect the presence of a Stern layer at the electrode surfaces to focus on the simplest case of discharging dynamics. The PNP equations consist of equations for the flux of ions driven by diffusion and migration, a charge conservation equation, and Poisson's equation relating the gradient of the electric field to the local charge density. The

cell is thin in the $\hat{x}$ direction (Fig. 1) but wide and long in the $\hat{y}$ and $\hat{z}$ directions. Hence, we assume that the transport is one dimensional in the $\hat{x}$ direction. The flux density of cations, $\hat{j}_p$, is

$$\hat{j}_p = -\hat{D}\frac{\partial \hat{p}}{\partial \hat{x}} - \frac{\hat{D}\hat{q}}{\hat{k}_B\hat{T}}\hat{p}\frac{\partial \hat{\phi}}{\partial \hat{x}}, \tag{1}$$

where $\hat{p}$ is the cation concentration, $\hat{\phi}$ is the electric potential, and $\hat{D}$ is the diffusivity of the ions, assuming equal diffusivity. The flux density of anions $\hat{j}_n$ is

$$\hat{j}_n = -\hat{D}\frac{\partial \hat{n}}{\partial \hat{x}} + \frac{\hat{D}\hat{q}}{\hat{k}_B\hat{T}}\hat{n}\frac{\partial \hat{\phi}}{\partial \hat{x}}. \tag{2}$$

The charge conservation equations are

$$\frac{\partial \hat{p}}{\partial \hat{t}} = -\frac{\partial \hat{j}_p}{\partial \hat{x}} \quad \text{and} \quad \frac{\partial \hat{n}}{\partial \hat{t}} = -\frac{\partial \hat{j}_n}{\partial \hat{x}}. \tag{3}$$

Poisson's equation is

$$\frac{\partial^2 \hat{\phi}}{\partial \hat{x}^2} = -\frac{\hat{q}}{\hat{\varepsilon}}(\hat{p} - \hat{n}). \tag{4}$$

The boundary conditions include no flux conditions for the ions at the electrode-electrolyte interface,

$$\frac{\partial \hat{p}}{\partial \hat{x}} = -\frac{\hat{q}}{\hat{k}_B\hat{T}}\hat{p}\frac{\partial \hat{\phi}}{\partial \hat{x}} \quad \text{and} \quad \frac{\partial \hat{n}}{\partial \hat{x}} = \frac{\hat{q}}{\hat{k}_B\hat{T}}\hat{n}\frac{\partial \hat{\phi}}{\partial \hat{x}}, \quad \text{at } \hat{x} = \pm\hat{L}. \tag{5}$$

The electric potential $\hat{\phi}(\hat{x} = \pm\hat{L}) = 0$ at the electrode interfaces for $\hat{t} > 0$. At $\hat{t} < 0$, the cell is at steady state following the charging process driven by a voltage $\hat{V}$, so the charging steady state solution is the initial condition for discharging. In the linear and weakly nonlinear regime, we use Bazant et al.'s [9] steady state solutions as the initial condition. In the strongly nonlinear regime, we solve the PNP equations during charging numerically and use the numerical solution when the current reaches zero (within an error tolerance) as the initial condition for discharging.

We non-dimensionalize the above equations by normalizing length $\hat{x}$ by $\hat{L}$; the electric potential $\hat{\phi}$ by $\hat{V}_T$; and ion densities $\hat{p}$ and $\hat{n}$ by $\hat{c}_0$, the initial uniform ion concentration before charging. Bazant et al. [23] show that the relevant timescale for the exponential decay in the current during charging in the linear regime is the RC time, $\hat{t} \sim \hat{L}\hat{\lambda}_D/\hat{D}$,
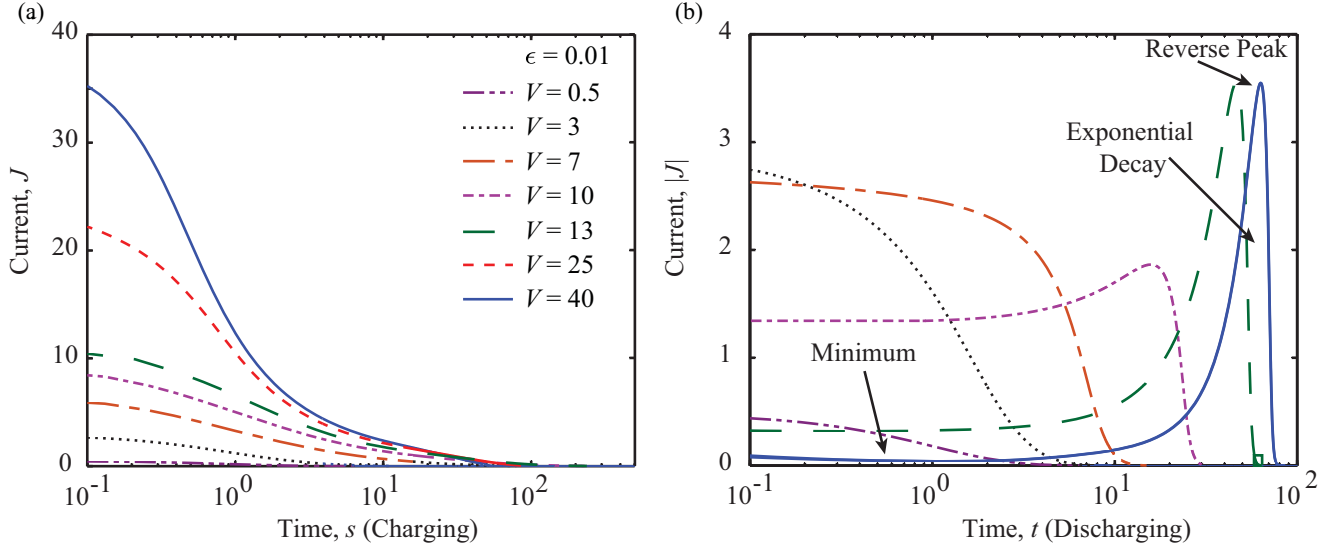
FIG. 2. Magnitude of the current resulting from step changes in voltage at $\epsilon = 0.01$. Time is scaled by the RC timescale. (a) The applied voltage is turned on at $s = 0$. The current decays monotonically towards zero during charging. (b) The applied field is switched off at $t = 0$. At low voltages $V = 0.5, 3, 7$, the magnitude of the current decreases monotonically towards zero during discharging. At larger voltages, $V = 10, 13, 25, 40$, the magnitude of the current decreases to a minimum, then reverses and increases to reach a maximum, the reverse peak, followed by a monotonic decay towards zero. At large voltage, $V = 25, 40$ the current appears to saturate; the curves for $V = 25, 40$ overlap.

where $\hat{\lambda}_D$ is the Debye length. Two dimensionless groups emerge: the dimensionless Debye length $\epsilon = \hat{\lambda}_D / \hat{L}$ and the dimensionless applied voltage $V = \hat{V} / \hat{V}_T$. These two groups fully characterize the charging and discharging dynamics, and remain constant throughout the charging-discharging cycle. Recall, all unhatted variables are dimensionless. The resulting dimensionless charge conservation equations (3), rewritten in terms of the mean salt concentration $c = \frac{1}{2}(p + n)$ and half the charge density $\rho = \frac{1}{2}(p - n)$ are

$$\frac{\partial c}{\partial t} = \epsilon \frac{\partial^2 c}{\partial x^2} + \epsilon \frac{\partial}{\partial x}\left(\rho \frac{\partial \phi}{\partial x}\right)$$

$$\text{and} \quad \frac{\partial \rho}{\partial t} = \epsilon \frac{\partial^2 \rho}{\partial x^2} + \epsilon \frac{\partial}{\partial x}\left(c \frac{\partial \phi}{\partial x}\right), \quad (6)$$

where $\epsilon = \lambda_D / L \ll 1$ at the experimentally relevant thin double layer limit. The dimensionless form of Poisson's equation (4) is

$$-\epsilon^2 \frac{\partial^2 \phi}{\partial x^2} = \rho. \quad (7)$$

The dimensionless boundary conditions are

$$\frac{\partial \rho}{\partial x} = -c \frac{\partial \phi}{\partial x}, \quad \frac{\partial c}{\partial x} = -\rho \frac{\partial \phi}{\partial x}, \quad \text{and} \quad \phi = 0 \text{ at } x = \pm 1. \quad (8)$$

After solving for the concentration, charge density, and potential, the external current can be calculated from Gauss' law [23]. The external current is equal to the change in the electric field with time at the electrode surface, and can be calculated at either electrode due to symmetry in the electric field about $x = 0$. The dimensionless expression for the current J in the external circuit is

$$J = \epsilon \frac{\partial^2 \phi}{\partial x \partial t}\bigg|_{x=-1}, \quad (9)$$

where J is scaled by $2\hat{A}\hat{D}\hat{c}_0\hat{q}/\hat{L}$, and $\hat{A}$ is the surface area of the electrode.

III. NUMERICAL SOLUTION TO THE PNP EQUATIONS

The dimensionless PNP equations (6),(7) along with the boundary conditions (8) are solved numerically using MATLAB's pdepe solver, a finite-difference based, initial-value problem solver. The numerical solution provides insight on the behavior of the system at a range of applied voltages V and Debye lengths ϵ to guide our asymptotic analyses. The experimental and numerical results from Kornilovitch and Jeon [13] indicate that as the applied voltage increases for a fixed value of $\epsilon \ll 1$, the dynamics transition from linear to nonlinear, indicated by the appearance of a reverse peak in the magnitude of the current. We solved the PNP equations for $\epsilon = 0.01$ and voltages ranging from $V = 0.5$–40 in Fig. 2.

Here, the time during charging is s, where the applied voltage undergoes a step change from $\phi(\pm 1) = 0$ to $\phi(\pm 1) = \pm V$ at $s = 0$. The current during charging decays monotonically for all V. The time variable during discharging is t, where the applied voltage is switched off at $t = 0$, so that $\phi(\pm 1) = 0$ for $t > 0$. After the applied voltage is switched off, the external current ultimately decays in magnitude towards zero at steady state. However, the decay is only monotonic at lower applied voltages ($V = 0.5, 3, 7$). At $V \geqslant 10$, the magnitude of the current reaches a minimum before reversing towards a maximum referred to as the reverse peak. As the applied voltage increases further ($V = 25, 40$), the current appears to saturate, meaning that the reverse peak does not shift with increasing voltage. After the reverse peak, the current decays exponentially in time for all voltages, with a similar slope. This indicates that the time scale for the decay in the current at a specific value of ϵ is constant across a range of applied voltages. We aim to identify the charge transport dynamics that

result in the asymmetry between charging and discharging in the nonlinear regimes, and the limiting factor leading to saturation of the reverse peak.

IV. LINEAR DYNAMICS

We follow the analysis of Bazant *et al.* [9] describing the ion dynamics during charging to solve for the charge density and potential profiles during the discharging process. At low applied voltages where the applied voltage is less than the thermal voltage, formally $V \ll 1$, all quantities are written as a regular expansion in V, resulting in $c = c_0 + V c_1 + O(V^2)$, $\rho = V \rho_1 + O(V^2)$, and $\phi = V \phi_1 + O(V^2)$. The expansions are inserted in Eq. (6), yielding

$$\frac{\partial^2 c_1}{\partial x^2} = 0. \tag{10}$$

Integrating Eq. (10) results in $c_1(x) = a(t)x + b(t)$. The no-flux boundary conditions (8) to $O(V)$, $\frac{\partial c_1}{\partial x} = 0$ at $x = \pm 1$, require that $a = 0$. Finally, the integral of the concentration $\int_0^1 c_1 dx = 0$, as the number of ions is conserved in the absence of Faradaic reactions, thus $b = 0$ and $c_1 = 0$. The concentration is thus equal to the initial concentration in the electrolyte, c_0 through $O(V)$. The $O(V)$ charge density evolves according to the linear Debye-Falkenhagen equation [24], written in terms of $\rho = V \rho_1$ as

$$\frac{1}{\epsilon} \frac{\partial \rho}{\partial t} = \frac{\partial^2 \rho}{\partial x^2} - \frac{1}{\epsilon^2} \rho. \tag{11}$$

The initial condition for this equation is the steady state charge density ρ_{ss} after charging [9],

$$\rho_{ss}(x) = -V \frac{\sinh(x/\epsilon)}{\sinh(1/\epsilon)}. \tag{12}$$

The linearized boundary conditions (8) are

$$\frac{\partial \rho}{\partial x} = -\frac{\partial \phi}{\partial x}, \text{ at } x = \pm 1. \tag{13}$$

We solve Eq. (11) by a Laplace transform $\mathcal{L}$ in time, where $\mathcal{L}(f(t)) = \check{f}(T)$ and T denotes the Laplace variable. The Laplace-space quantities are denoted by a check superscript. The Laplace transformed Debye-Falkenhagen equation is

$$\left(\frac{T}{\epsilon} \check{\rho} + \frac{V}{\epsilon} \frac{\sinh(x/\epsilon)}{\sinh(1/\epsilon)} \right) = \frac{\partial^2 \check{\rho}}{\partial x^2} - \frac{1}{\epsilon^2} \check{\rho}. \tag{14}$$

Assuming antisymmetry in the charge density about $x = 0$, the solution is

$$\check{\rho} = A \sinh(mx) - \frac{V\epsilon}{m^2\epsilon^2 - 1} \frac{\sinh(x/\epsilon)}{\sinh(1/\epsilon)}, \tag{15}$$

where $m = \sqrt{T/\epsilon + 1/\epsilon^2}$ and $A(T)$ is an as yet unknown function of T. Inserting Eq. (15) into the Laplace transform of Poisson's equation (7) and integrating once yields

$$\frac{\partial \check{\phi}}{\partial x} = -\frac{A}{m\epsilon^2}[(m^2\epsilon^2 - 1)\cosh(m) + \cosh(mx)]$$
$$+ \frac{V}{m^2\epsilon^2 - 1} \frac{\sinh(x/\epsilon)}{\sinh(1/\epsilon)}. \tag{16}$$

By requiring the potential $\phi(t,0) = 0$ due to antisymmetry, and applying the boundary conditions (13) we find that

$$A(T) = \frac{m^2\epsilon^3 V}{(m^2\epsilon^2 - 1)[m(m^2\epsilon^2 - 1)\cosh(m) + \sinh(m)]}. \tag{17}$$

Integrating Eq. (16) yields the Laplace transform of the electrical potential,

$$\check{\phi} = -\frac{A}{m^2\epsilon^2}[m(m^2\epsilon^2 - 1)x\cosh(m) + \sinh(x/\epsilon)]$$
$$+ \frac{V\epsilon}{m^2\epsilon^2 - 1} \frac{\sinh(x/\epsilon)}{\sinh(1/\epsilon)}. \tag{18}$$

At long times, $T \to 0$, the charge density (15) decays exponentially. Specifically, at this limit, the charge density can be expanded as

$$\check{\rho}_{S\to0} = \frac{\frac{V}{2}\operatorname{csch}(1/\epsilon)[x\cosh(x/\epsilon) + (2\epsilon - 3\coth(1/\epsilon))\sinh(x/\epsilon)]}{1 + T\coth(1/\epsilon)} + O(T). \tag{19}$$

This Laplace-space equation for the charge density at long times can be inverted to yield

$$\rho_{t\to\infty} = \frac{V}{2}\operatorname{sech}(1/\epsilon)[x\cosh(x/\epsilon) + (2\epsilon - 3\coth(1/\epsilon))$$
$$\times \sinh(x/\epsilon)]\exp(-t\tanh(1/\epsilon)). \tag{20}$$

This reveals that the time scale for charge density relaxation in the linear regime is

$$\tau = \coth(1/\epsilon), \tag{21}$$

where time is scaled by the *RC* time, $\hat{L}\hat{\lambda}_D/\hat{D}$. This agrees with the timescale found by Bazant *et al.* [9] for the charging process. For comparison, in the charging case, the Laplace transform of the charge density is $\check{\rho}_{\text{charge}} = TA\sinh mx$, where A is given in Eq. (17).

Equations (15) and (18) for the charge density and electric potential in Laplace space, alongside Eq. (17) for the parameter A, can be inverted numerically using an Euler summation method [25]. The numerically inverted solution for charge density is compared to the long-time solution (20) and numerical solution to Eqs. (6)–(8) in Fig. 3 for $V = 0.5$ and $\epsilon = 0.05$. The agreement between numerics and the Laplace transform solutions indicates that the assumption that the concentration is uniform and equal to one throughout the cell is valid at low voltages.

In the linear regime, the external current during charging and discharging is antisymmetric. However, the potential and charge density profiles are not. In Fig. 4, we show the potential and charge density during charging and discharging. At s_1
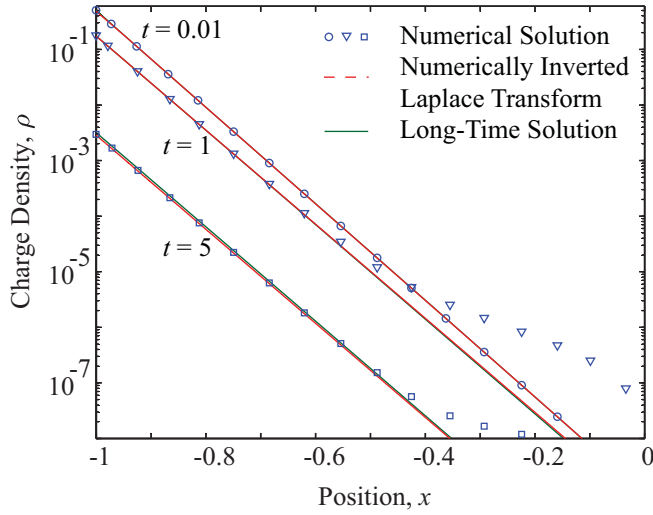
FIG. 3. The numerically inverted Laplace transform solution (15) (dash) for the charge density and the long-time solution for the charge density (20) (line) at $V = 0.5$ and $\epsilon = 0.05$ are compared to the numerical solution of the PNP equations (6)–(8) (circle) at $t = 0.01, 1, 5$. Only the cathodic half of the cell is shown.

and t_1, the magnitude of the current $|J| = 0.25$; at s_2 and t_2, $|J| = 0.05$. The two pairs of curves show that, at the same current magnitude in the charging and discharging cycle, the potential and charge density profiles are not equivalent. This is counterintuitive given the antisymmetry of the external current [Fig. 4(c)]. At $t_1 = s_1$, the current is equal to $|J| = V/2$, or half of its maximum value $|J(t = 0)| = V$, indicating that the charging and discharging processes are at the halfway point. As time continues the charge density during charging increases, while the discharging charge density decreases, emphasizing the asymmetry of the charging and discharging dynamics. When the applied voltage at the electrode switches to zero,
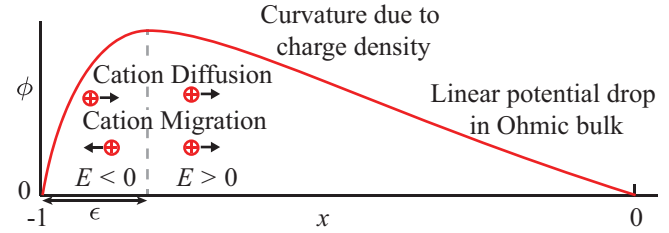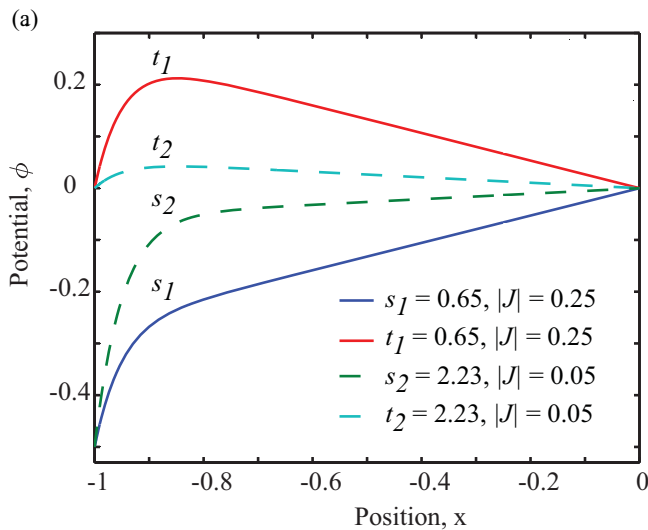
FIG. 5. During discharging, the potential is zero at the electrode and the midpoint. The curvature in the potential is due to the charge density in the double layer according to Poisson's equation (7). The electric field is negative in the double layer and positive in the bulk. Cation migration and diffusion oppose each other in the double layer, whereas they do not in the bulk.

the potential profile rapidly switches in response [Fig. 4(a)], to the potential profile shown in the schematic in Fig. 5. The maximum in potential is located at an $O(\epsilon)$ distance from the electrode, where the charge density in the double layer causes curvature in the potential according to Poisson's equation (7). In the double layer, the migration of cations is directed towards the electrode due to the negative electric field, while cation diffusion is toward the midpoint of the cell driven by the steep drop in concentration from the double layer to the bulk. The potential is linear in the electroneutral bulk, where cation migration is towards the center. The potential profile also holds in the weakly nonlinear regime. In the strongly nonlinear regime, charge density in the bulk leads to curvature in the bulk potential [Fig. 9(b)] during discharging according to Poisson's equation (7).

V. WEAKLY NONLINEAR DYNAMICS

When the applied voltage is on the order of the thermal voltage, the salt concentration is not uniform throughout the cell. In order to screen the surface charge on the electrodes,
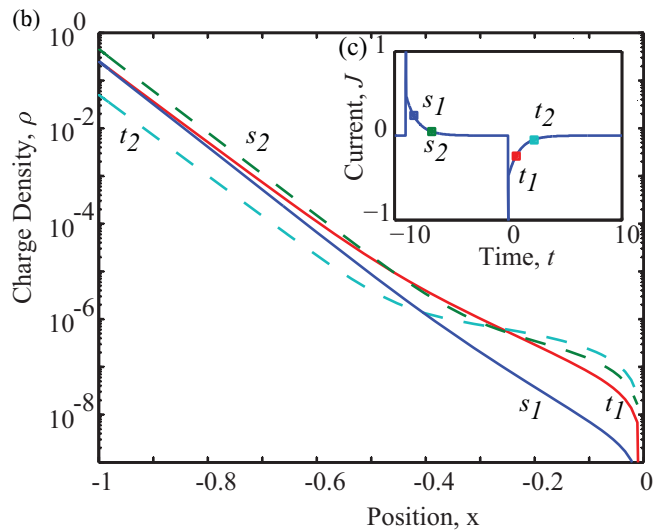
FIG. 4. The potential and charge density, from the numerical solution to the PNP equations, are plotted during charging and discharging at two pairs of times at which the current is equal in magnitude. Here, $\epsilon = 0.05$ and $V = 0.5$. At s_1 and t_1 (line), the current (c) is $|J| = 0.25$, while $|J| = 0.05$ at s_2 and t_2 (dash). Neither the potential (a) nor charge density (b) profiles match at a given magnitude of the current. Only the cathodic half of the cell is shown.

the thin double layers adsorb neutral salt from the bulk [24] at a concentration that depends nonlinearly on the applied voltage [26]. This nonlinear capacitance is characteristic of the weakly nonlinear regime [9]. To a first approximation, accumulation of ions in the thin double layer does not significantly deplete the bulk of ions, so the bulk salt concentration is $c = 1$ to leading order in ϵ. Bulk diffusion, accordingly, is negligible in this regime. To solve for the external current during discharging in this weakly nonlinear regime, we address the PNP equations (6)–(8) in the thin-Debye-layer limit, $\epsilon \to 0$. Equations (6)–(8) are singular as $\epsilon \to 0$, motivating the use of matched asymptotic expansions [27]. In the weakly nonlinear regime, the electrolytic cell comprises the double layer, or inner region of width $x \sim O(\epsilon)$, adjacent to the electrode and the bulk, or outer region of width $x \sim O(1)$, centered around the midpoint of the cell. The boundary conditions (8) apply at the literal electrode-electrolyte interface.

Bazant *et al.* [9] apply matched asymptotics to the PNP equations (6),(7) for charging in the weakly nonlinear regime. In the bulk, the position $x \sim O(1)$ as $\epsilon \to 0$. Bazant *et al.* [9] perform regular expansions in ϵ in the bulk, and coordinate rescaling in the inner region, the Debye layer. The Debye layer is shown to have a quasi-equilibrium Gouy-Chapman structure. Regular expansions in ϵ in the bulk are inserted into Eqs. (6),(7), yielding the leading order bulk concentration, $c_c = 1$, an asymptotically small charge density ρ_c, and bulk potential

$$\phi_c = j_c(s)x, \qquad (22)$$

where j_c is the current density to leading order in ϵ. The subscript c refers to the charging process. The position, x is the outer coordinate where $x = \pm 1$ corresponds to the outer edge of the inner region. Matching between the double layer and the bulk shows that the current density j_c is asymptotic to the external current J and is given by the solution to the differential equation [9]

$$C_c \frac{dj_c}{ds} = -j_c \quad \text{and} \quad j_c(s = 0) = V, \qquad (23)$$

where C_c is the capacitance of the double layer,

$$C_c = \cosh\left[(j_c - V)/2\right]. \qquad (24)$$

The capacitance (24) is a function of the total voltage and the flux of ions j_c from the bulk to the double layer. As ions flow from the bulk to the double layer during charging, the capacitance increases. It can be shown that the current density j_d during discharging is similarly given by the solution of

$$C_d \frac{dj_d}{dt} = -j_d \quad \text{and} \quad j_d(t = 0) = V, \qquad (25)$$

where $C_d = \cosh(j_d/2)$ is the differential capacitance of the double layer. The initial condition for discharging can be calculated from $\phi_d = j_d(t)x$, where the potential is $\phi_d(0, -1) = -V$ at $x = -1$. This shows that the potential drop in the bulk is linear, which is consistent with the applied potential at $V = 0.5$ in Fig. 4. The initial current is thus $j_d(0) = V$. With this initial condition, the implicit solution to Eq. (25) is

$$t = F_d(j_d) - F_d(V), \quad \text{where} \quad F_d(u) = -\int_0^u \frac{\cosh z/2}{z}\,dz. \qquad (26)$$

For comparison, the current in the charging case j_c, is given by the implicit solution to [9]

$$s = F_c(j_c - V), \quad \text{where} \quad F_c(u) = -\int_0^u \frac{\cosh z/2}{z + V}\,dz. \qquad (27)$$

The current during charging j_c is not antisymmetric to the discharging current j_d in the weakly nonlinear regime. As stated previously, the current density j_d is asymptotic to the external current J. In Fig. 6 we compare the numerical solution to Eq. (26) for the current density j_d to the numerical solution to Eqs. (6)–(8) for the external current J and the numerical
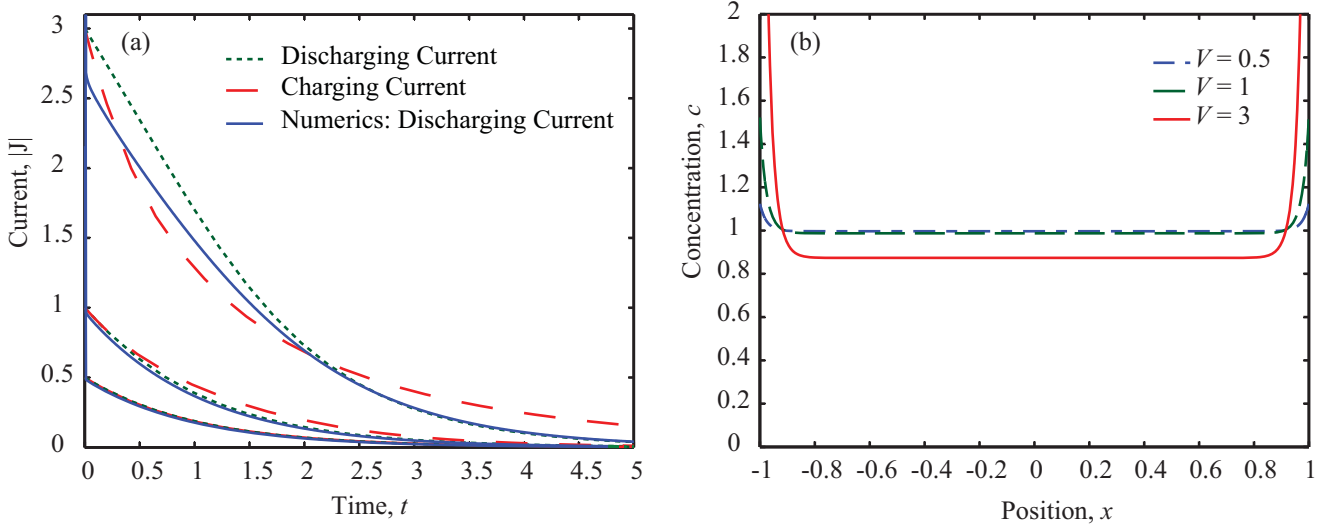
FIG. 6. (a) Current during discharging j_d (dot), given by Eq. (25), compared to the current during charging j_{0c} (dash), given by Eq. (27), and the numerically calculated current J (line) during discharging for three applied voltages, $V = 0.5, 1, 3$ and $\epsilon = 0.05$. (b) Concentration at time $t = 0$ for $V = 0.5, 1, 3$. At $V = 3$, the bulk concentration is not equal to unity due to salt adsorption in the double layer and ion depletion in the bulk, which invalidates the weakly nonlinear analysis.

solution to Eq. (27) for the current density during charging j_c at $V = 0.5, 1, 3$ and $\epsilon = 0.05$. At low applied voltages $V \ll 1$ (linear regime), the current density during charging, discharging, and the external current match, as expected. However, deviations arise at $V = 1$, and are strongly apparent at $V = 3$. First, when comparing the charging and discharging current densities in Fig. 6, the discharging process occurs at a more rapid pace than charging. During charging, migration and diffusion oppose each other during the formation of the double layers. Conversely, during discharging the bulk potential and diffusion fluxes both promote the movement of cations from the electrode to the bulk, as depicted in Fig. 5. Secondly, $J \neq V$ at $t = 0$. Instead, the current $J < 3$ initially for $V = 3$. To leading order, the flux $j_d = c_0 V$ and $c_0(x) = 1$ for all x at $t = 0$. Figure 6(b) shows that the bulk concentration at $V = 3$ and $t = 0$ is lower than 1, $c_0 \sim 0.87$. If we insert this bulk concentration $c_0 = 0.87$ and $V = 3$ into $j_d = c_0 V$, we find $j_d = 2.61$. At $t = 0$, $|J| = 2.68$, according to the numerical solution for J at $V = 3$, so the correction in the bulk concentration c_0 captures the decrease in current at $t = 0$. At long times for $V = 3$, the external current J matches j_d because $c_0 \to 1$ as $t \to \infty$, thus the effect of initial bulk depletion on j_d does not play a role as $t \to \infty$. We conclude that the drop in the magnitude of the external current at $t = 0$ is due to an increase in the adsorption of ions in the double layer, balanced by depletion of ions in the bulk.

The weakly nonlinear analysis breaks down when the total concentration in the double layer, $c_D \sim c_0 \epsilon \exp V$ to $O(\epsilon)$ according to the Gouy-Chapman model [28,29], is on the order of the concentration in the bulk, c_0. This occurs at an applied voltage (normalized by V_T) $V \sim \ln 1/\epsilon$. At $\epsilon = 0.05$, the breakdown is predicted at $V = 3$, in agreement with the results in Fig. 6. Bazant *et al.* [9] define a similar limit for the weakly nonlinear analysis during charging; namely, $4\epsilon \sinh^2(V/4) \ll 1$.

The weakly nonlinear analysis presented here captures the asymmetry in the current between charging and discharging stemming from nonlinear capacitance in the double layer. However, the analysis does not predict a reversal in the current during discharging. Indeed, the current is monotonic. We must therefore conclude that the non-monotonic current at higher voltages is due to bulk diffusion, indicating that the reversals in the current must occur on the diffusion timescale. In the following section, we numerically investigate the effects of bulk depletion and diffusion on the current at large voltages.

VI. STRONGLY NONLINEAR DYNAMICS

When the applied voltage is larger than $V \sim \ln 1/\epsilon$, the double layers adjacent to the electrodes deplete the bulk of ions during charging. The weakly nonlinear analysis assumed that the bulk concentration was equal to the initial uniform concentration; at larger voltages, this assumption breaks down, indicating a transition to the strongly nonlinear regime. The strongly nonlinear regime is characterized by the development of a "reverse peak", or a maximum in the magnitude of the current during the discharging process, due to neutral salt desorption from the double layer to the bulk.

Recall, before the electric field is switched on, the ions are uniformly distributed throughout the cell. After the field is
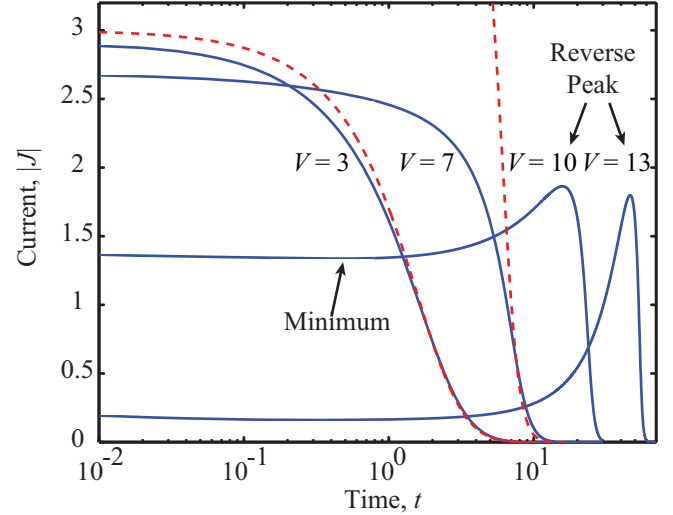
FIG. 7. The current at a fixed double layer thickness, $\epsilon = 0.01$, shows the development of the reverse peak as V increases. The current calculated from the numerical solution to the PNP equations is compared to the weakly nonlinear current j_d (dash) for $V = 3$ and $V = 7$. The transition from weakly to strongly nonlinear occurs at $V \sim -\ln 0.01 = 4.7$.

applied, the ions separate to form double layers adjacent to the electrodes. Once the system reaches steady state, the external current decays to zero, and the applied field is switched off. After an initial spike, the magnitude of the current decays to a minimum. After this point, ions from the double layer diffuse and migrate into the bulk, leading to an acceleration in the current to a reverse peak, before the current magnitude decays to zero. The current during discharging is shown in Fig. 7 for $\epsilon = 0.01$ and applied voltages between $V = 3$ and $V = 13$, from which this behavior is clearly observed. The $V = 3$ case is in the weakly nonlinear regime. The current is compared to the current density j_d (26) calculated from the weakly nonlinear analysis, which qualitatively matches the numerical results. The weakly nonlinear asymptotics deviate from the numerical solution at short times due to bulk depletion, as discussed in Sec. V. As the voltage increases to $V = 7$, the weakly nonlinear analysis no longer matches the current, but the latter is still monotonic (Fig. 7). As the voltage increases further ($V = 10, 13$), the reverse peak emerges and becomes more pronounced in comparison to the minimum in the magnitude of the current.

The asymmetry between the charging and discharging processes is highlighted by the development of the reverse peak. In order to better understand the origin of the reverse peak, we investigate the current on three timescales relevant to the discharging dynamics. The largest of these is the diffusion time, $\hat{t}_D = \hat{L}^2/\hat{D}$, followed by the RC time $\hat{t}_{RC} = \hat{L}\hat{\lambda}_D/\hat{D}$, and finally the double layer relaxation time, $\hat{t}_\lambda = \hat{\lambda}_D^2/\hat{D}$.

In Fig. 8, the current is plotted for pairs of V and ϵ that fall within the strongly nonlinear regime but do not completely deplete the bulk of salt during charging. The emergence of the reverse peak in cases where the concentration in the bulk is larger than $O(\epsilon)$, as shown in Fig. 9(c) for $V = 13$ and $\epsilon = 0.01$, indicates that total charge separation is not required

(a)

(b)

(c)
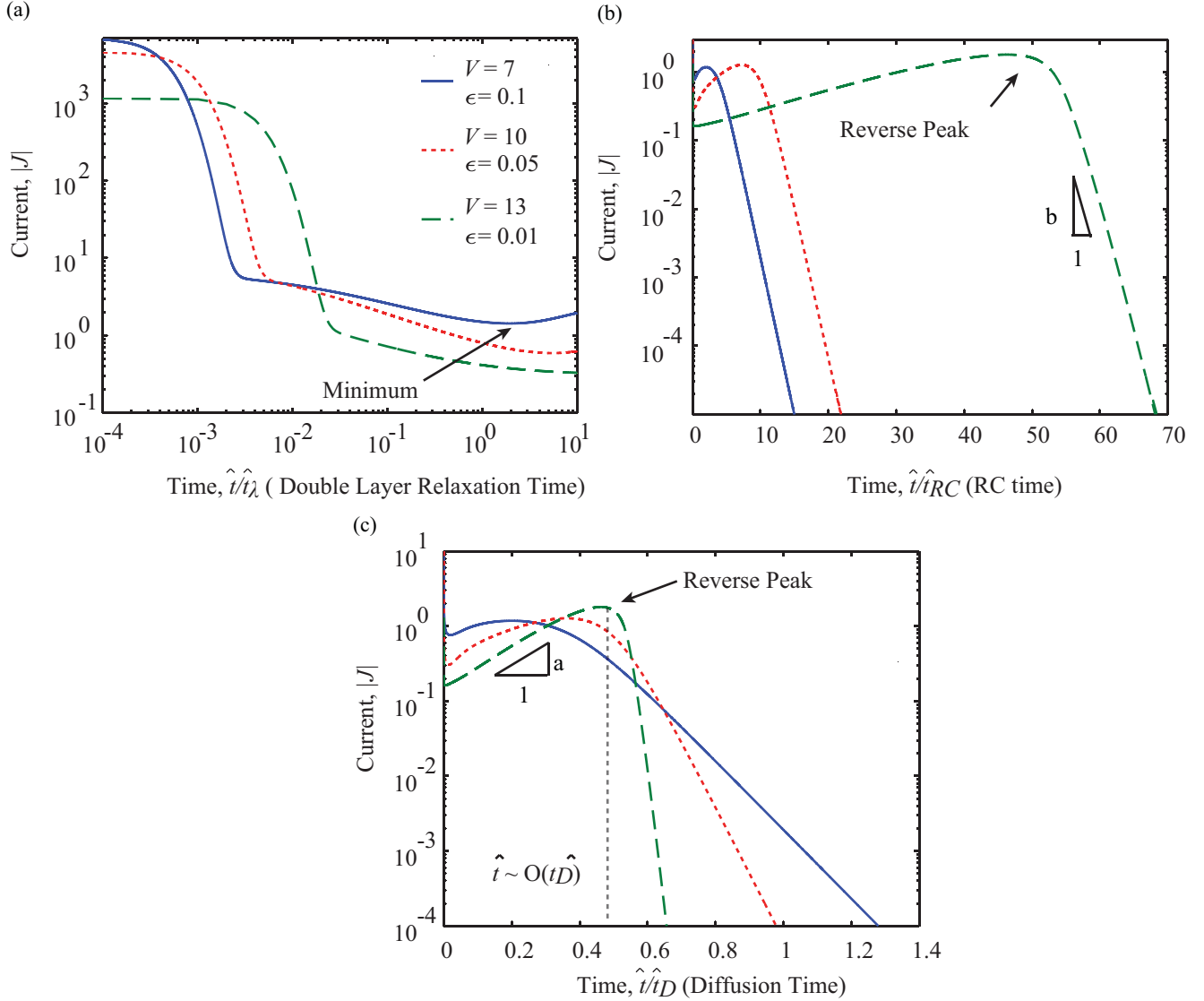
FIG. 8. The current during discharging is scaled by three timescales: (a) the double layer relaxation timescale, (b) the RC timescale, and (c) the diffusion timescale. The three cases shown here, $\epsilon = 0.1$ and $V = 7$, $\epsilon = 0.05$ and $V = 10$, $\epsilon = 0.01$ and $V = 13$, are in the strongly nonlinear regime after the development of the reverse peak.

for a reverse peak in the current. Figure 8(a), scaled on the double layer relaxation time, shows the initial spike in current, followed by a minimum in the current that occurs at an $O(1)$ time. Time is plotted on a log-log scale here. On this scale, the current is approximately linear leading up to the minimum in current magnitude.

In Fig. 8(b), time is scaled by the RC time $\hat{t}_{RC}$ for three values of ϵ and applied voltage V. When plotted on a log-linear scale, the decay in current after the reverse peak is linear, corresponding to an exponential decay in the current at long times. The timescale b for the exponential decay $J \sim \exp(-bt)$ is $O(1)$, indicating that the decay is occurring on the RC time $\hat{t}_{RC}$. This is consistent with the exponential decay in the current in the linear regime (21), where $b = \coth(1/\epsilon) \sim 1$ for small ϵ. Finally, the current is rescaled on the diffusion time $\hat{t}_D$ in Fig. 8(c). The time at which the reverse peak occurs is on the order of the diffusion time, indicating that the rapid growth in the current before the reverse peak is driven by the

diffusion of ions from the double layer to the bulk (Fig. 9). The exponential increase in the current magnitude is on the timescale a, where $J \sim \exp(at)$ and $a \sim O(1)$ preceding the reverse peak.

While the current during discharging provides insight into the dynamics of the cell, the concentration and potential profiles enable a closer look. Figure 9 shows the evolution of the current magnitude $|J|$, the potential, ϕ, concentration c, and charge density ρ for $\epsilon = 0.01$ and $V = 13$ initially, at the minimum and maximum in current. The cathodic half of the cell is shown in Fig. 9; equivalent dynamics occur in the anodic half.

Immediately after the applied field is switched off, the potential at the electrode switches from $-V$ to 0. Charge density causes curvature in the potential, according to Poisson's equation (7). At $t = 0$, the large, positive charge density in the double layer is reflected in an increase in potential. As depicted in Fig. 5, the maximum in potential is outside of
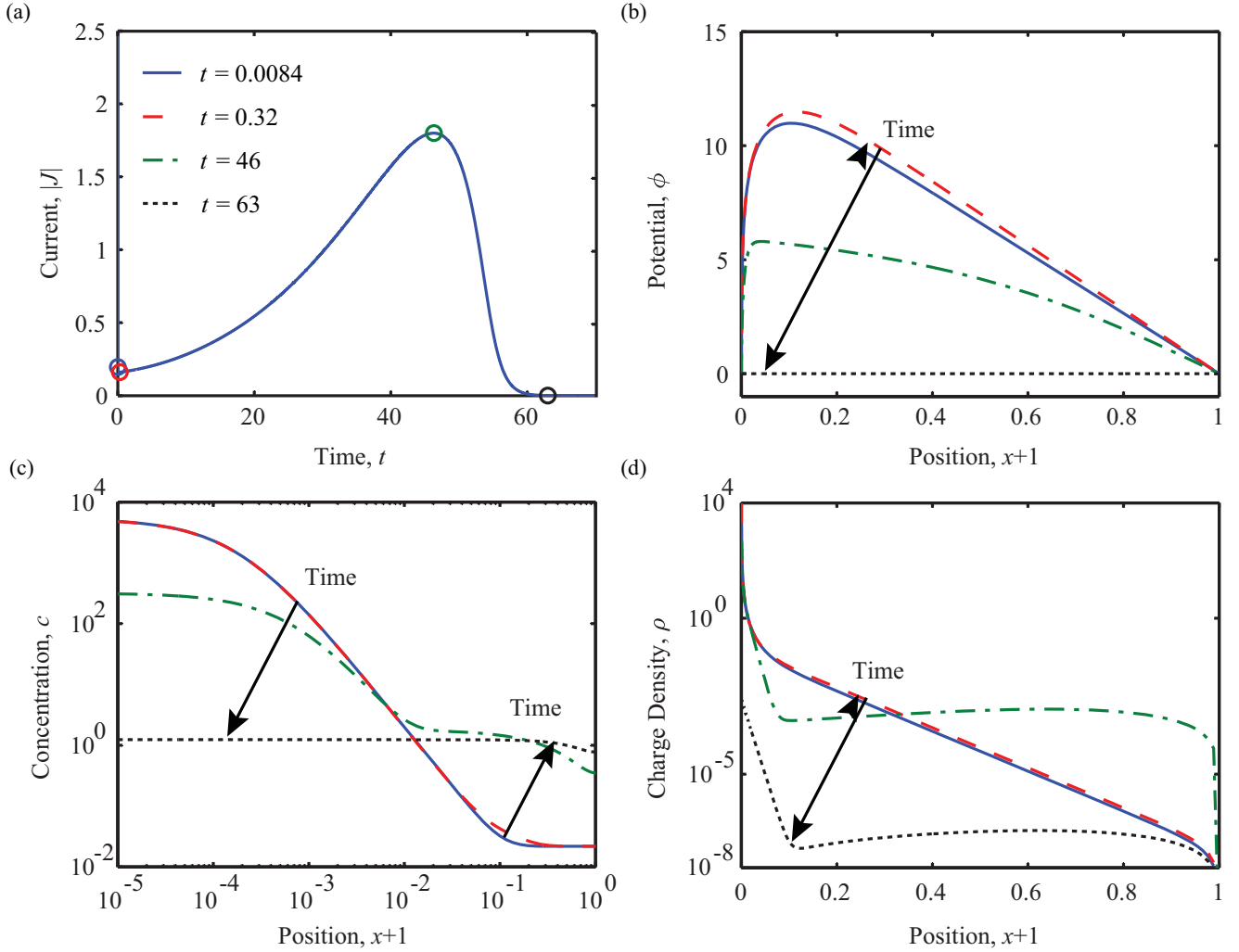
FIG. 9. The discharging dynamics for $V = 13$ and $\epsilon = 0.01$ are shown at multiple times corresponding to the extrema in the current: current (a), electric potential (b), concentration (c), and charge density (d). Position is plotted as $x + 1$ to allow for a log scale in x in (b), (c), and (d).

the double layer, where the charge density rapidly decays to zero. Initially, cations are concentrated in the double layers and depleted in the bulk [Fig. 9(c)]. From the first time-point to the second time-point, the latter corresponding to a minimum in the magnitude of the current, anions from the bulk of the cell migrate towards the maximum in potential, briefly increasing the charge density and potential, as indicated by the small arrows in Figs. 9(b) and 9(d). From the minimum in current ($t = 0.32$) to the reverse peak ($t = 46$), cations from the double layer diffuse and migrate into the bulk driven by strong concentration gradients, decreasing the concentration at the electrode, increasing the bulk concentration, and yielding an exponential rise in the magnitude of the current with time [Figs. 9(a) and 9(c)]. The charge density decreases in the bulk as both cations and anions enter, leading to a drop in the potential. As time approaches $t = 46$, the concentration gradient weakens, and the bulk concentration reaches O(1). Following the reverse peak, the cell behavior can be described by a linear RC circuit: the bulk resembles an Ohmic resistor in series with the double layer, represented as a linear capacitor. Accordingly, at times after the reverse peak, the current decays exponentially on the RC timescale, as shown in Fig. 8, until the

concentration profile is uniform and the current reaches zero. This is akin to the linear dynamics in Sec. IV. It is evident that the reverse peak is due to the onset of bulk depletion.

VII. REVERSE PEAK SATURATION AT VERY LARGE VOLTAGE

At larger voltages, $V \geqslant 25$ at $\epsilon = 0.01$, the discharging current appears to saturate (Fig. 2). This saturation is due to total charge separation and complete bulk depletion of salt during charging. In Fig. 10, the magnitude of the current at the reverse peak and the time of the reverse peak scaled by the diffusion time are plotted against $\ln \epsilon$ at voltages $V = 15, 20, 30, 40$, and 55. It is evident from the overlap in data points at $V \geqslant 30$ that the reverse peak has saturated in time and current magnitude, whereas at $V = 15$ and 20 the peak is shifting in time despite saturation in the magnitude of the current at the reverse peak. The current magnitude J_p and time of the reverse peak t_p scale as $\ln 1/\epsilon$. Therefore, we fit J_p and t_p for $V = 55$ to the expression $a \ln 1/\epsilon + b$ using the data points for $\epsilon = 0.001$ through 0.01. The resulting expressions
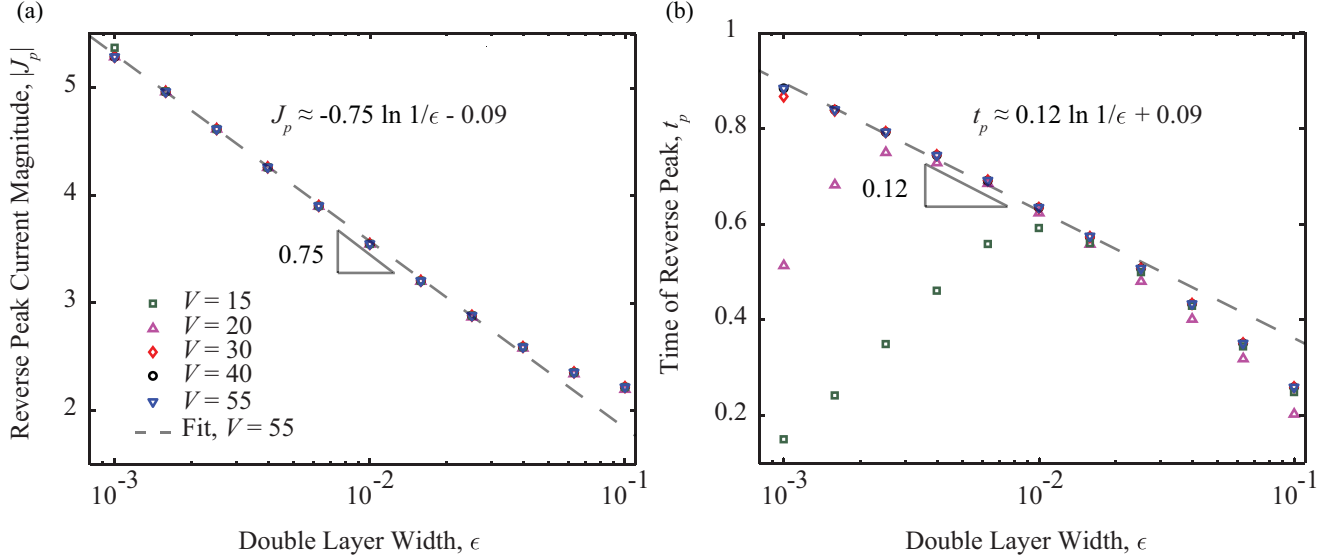
FIG. 10. The magnitude of reverse peak in the current (a) and the time of the reverse peak (b) scaled on the diffusion time are plotted at $V = 15, 20, 30, 40$, and 55 on a log scale in ϵ, demonstrating that both scale as $\ln 1/\epsilon$ to leading order. The line of best fit (dash) is fit to the peak current and time at $V = 55$ for $\epsilon = 0.001$ through 0.01.

for the peak current J_p and peak time t_p are

$$J_p = -a_j \ln 1/\epsilon - b_j \quad \text{and} \quad t_p = a_t \ln 1/\epsilon + b_t, \quad (28)$$

where $a_j = 0.755 \pm 0.005$, $b_j = 0.085 \pm 0.03$, $a_t = 0.116 \pm 0.004$, and $b_t = 0.093 \pm 0.02$. The error in these constants is the standard deviation of the points from the fitted expressions. The expression for the peak current (28) can be re-dimensionalized as

$$\hat{J}_p = (-a_j \ln 1/\epsilon - b_j)\frac{\hat{A}_0 \hat{D}}{\epsilon^2}, \quad (29)$$

where $\hat{A}_0 = \hat{A}\hat{\epsilon}\hat{k}_B\hat{T}/\hat{q}\hat{L}^3$. The dimensional peak time is

$$\hat{t}_p = (a_t \ln 1/\epsilon + b_t)\frac{\hat{L}^2}{\hat{D}}. \quad (30)$$

The correlations (29) and (30) can be used to infer the charge carrier diffusivity $\hat{D}$ and concentration $\hat{c}_0$ from experiments. To perform this experiment, the electrolytic cell should be discharged at a sufficiently large voltage $\hat{V}$ such that the reverse peak saturates in current and time. Equation (30) can be solved for diffusivity,

$$\hat{D} = (a_t \ln 1/\epsilon + b_t)\frac{\hat{L}^2}{\hat{t}_p}. \quad (31)$$

This expression can be inserted into Eq. (29), which is solved for ϵ. The result for ϵ is inserted into Eq. (31) to obtain $\hat{D}$. The charge carrier concentration $\hat{c}_0$ can be calculated from $\epsilon = 1/L\sqrt{\hat{\epsilon}\hat{k}_B\hat{T}/2\hat{q}^2\hat{c}_0}$. This is a single-point measurement to estimate diffusivity and charge carrier concentration; one only needs the value of $\hat{t}_p$ and $\hat{J}_p$.

We applied this method to Kornilovitch and Jeon's [13] experimental results for the saturated reverse peak in current in an OLOA 11000-doped, Isopar M system. Those experiments were performed in a 10 μm thick cell, with 0.5 wt.% OLOA 11000 at temperature $T = 10$ C. Figure 1 D in their paper

show a peak time of $\hat{t}_p = 1.63$ s and a peak current of $\hat{J}_p = -6.3 \times 10^{-8}$ A, at $\hat{V} = 8$ V. These values were inserted into Eqs. (29) and (30) to yield a diffusivity $\hat{D} = 3.2 \times 10^{-11}$ m^2/s, dimensionless Debye length $\epsilon = 0.024$, and charge carrier concentration $\hat{c}_0 = 37$ nmol/L. These values are consistent in magnitude with values predicted by Kornilovitch and Jeon's [13] method, $\hat{D} = 7 \times 10^{-12}$ and $\hat{c}_0 = 12.15$ nmol/L at $V = 1.16$ V. Their method was based firstly on estimating the skewness of the reverse peak for a range of charge carrier concentrations, and secondly integrating the discharging current over all times to obtain the charge carrier concentration. We emphasize that our approach requires only a single-point measurement.

VIII. CONCLUSIONS

This work was motivated by the asymmetry between the current during charging and discharging of an electrolytic cell, which has been experimentally observed [10–13]. This asymmetry arises when the applied voltage is on the order of the thermal voltage or larger. We analyzed the discharging process in three regimes defined by the applied voltage magnitude via asymptotic analysis and numerical methods. We derived asymptotic solutions for the current in the linear and weakly nonlinear regimes that can be directly applied to analyzing experimental data. For the strongly nonlinear regime, we identified three relevant timescales for discharging dynamics and the impact of bulk depletion on the emergence and ultimate saturation of the reverse peak.

The discharging dynamics are linear when the applied voltage is smaller than the thermal voltage. We solved the charge transport equations via Laplace transforms in the linear regime, where the concentration is uniform throughout the cell to leading order. We find that the timescale for the exponential decay in the current during discharging is the RC timescale, and that the current is anti-symmetric to the charging current.

Interestingly, the electric potential and charge density are not antisymmetric between charging and discharging. This can be attributed to a complementary diffusion and migration fluxes during discharging (Fig. 5), where both point towards the midpoint of the cell, compared to opposing diffusion and migration flux during charging.

At an applied voltage on the order of the thermal voltage, nonlinear capacitance in the double layers results in weakly nonlinear dynamics. We analyzed the weakly nonlinear dynamics via matched asymptotics for thin double layers and derived an asymptotic expression for the external current. The asymptotic current matches the current calculated from the numerical solution to the PNP equations provided $V \lesssim \ln 1/\epsilon$. At $V \sim \ln 1/\epsilon$, the asymptotic current deviates from the numerical solution at early times due to neutral salt adsorption in the double layers and depletion in the bulk, indicating a breakdown in the weakly nonlinear analysis. Our work shows that bulk depletion results in the emergence of the reverse peak in current. The reverse peak occurs on the diffusion timescale, indicating that the diffusion of ions from the double layer to the bulk drives the acceleration in current. The timescale for the exponential decay in the magnitude of the current following the reverse peak is the RC timescale. At long times, the discharging cell behaves as a linear RC circuit, and mimics the behavior of the linear regime. At very large voltage ($V \gg \ln 1/\epsilon$), the reverse peak saturates due to total depletion of the bulk salt during charging. We fit the current and time of the saturated reverse peak to develop expressions (29) and (30) correlating the peak current and time to ϵ and the charge carrier diffusivity $\hat{D}$. These correlations can be used to infer the value of these two parameters as well as the charge carrier concentration $\hat{c}_0$ from experiment, as we have demonstrated.

In this work, we solved the PNP equations for a binary, symmetric electrolyte. When the diffusivities of the ions are unequal, it can be shown that the decay in the external current in the linear regime is on the ambipolar RC time, $\hat{\lambda}_D \hat{L}/\hat{D}_a$. Here, $\hat{D}_a$ is the ambipolar diffusivity, $\hat{D}_a = 2D_1 D_2/(D_1 + D_2)$,

where D_1 and D_2 are the cation and anion diffusivities. Recall, the reverse peak occurs on the diffusion timescale. When the ions have unequal diffusivities, it is likely that multiple reverse peaks in the current will be observed at timescales corresponding to the diffusivity of the two species and the ambipolar diffusivity. This is an interesting problem for future work; charge carriers of opposite sign are not necessarily of equal size in surfactant doped non-polar fluids.

The PNP equations assume a dilute solution of non-interacting ions. This can lead to an unphysically large concentration of ions in double layers at large voltages. Kilic *et al.* [30,31] analyze the dynamics of a charging electrolytic cell at large voltage by incorporating the effects of steric hindrance of ions, via Bikerman's model [32]. Steric hindrance can be especially important for charge transport in doped nonpolar fluids as the charges are encapsulated in micelles. For reference, OLOA 1100 inverse micelles in dodecane are around 7 nM in diameter [20]. Kilic *et al.* [30,31] show that including steric hindrance via Bikerman's model limits the ion concentration in the double layers, which grows exponentially with voltage in the standard PNP equations. Note that more sophisticated theories of steric hindrance yield concentrations that do in fact grow with voltage, albeit at a much slower rate than predicted by PNP theory (see Gillespie [33] for a detailed discussion). In any case, with steric hindrance, the weakly nonlinear regime will extend to higher voltage than $V_T \ln 1/\epsilon$. The emergence of the reverse peak would likely be shifted to higher voltage using Bikerman's model [32]. This is an interesting problem for future work.

[1] John C. Berg, *An Introduction to Interfaces & Colloids: The Bridge to Nanoscience* (World Scientific, Singapore, 2010).

[2] P. M. Biesheuvel and A. Van der Wal, Membrane capacitive deionization, J. Membr. Sci. **346**, 256 (2010).

[3] P. M. Biesheuvel and M. Z. Bazant, Nonlinear dynamics of capacitive charging and desalination by porous electrodes, Phys. Rev. E **81**, 031502 (2010).

[4] T. Humplik, J. Lee, S. C. Ohern, B. A. Fellman, M. A. Baig, S. F. Hassan, M. A. Atieh, F. Rahman, T. Laoui, R. Karnik *et al.*, Nanostructured materials for water desalination, Nanotechnology **22**, 292001 (2011).

[5] T. Morimoto, M. Tsushima, M. Suhara, K. Hiratsuka, Y. Sanada, and T. Kawasato, Electric double-layer capacitor using organic electrolyte, in *MRS Proceedings* (Cambridge University Press, Cambridge, 1997), Vol. 496, p. 627.

[6] Celine Largeot, Cristelle Portet, John Chmiola, Pierre-Louis Taberna, Yury Gogotsi, and Patrice Simon, Relation between the ion size and pore size for an electric double-layer capacitor, J. Am. Chem. Soc. **130**, 2730 (2008).

[7] John Chmiola, Celine Largeot, Pierre-Louis Taberna, Patrice Simon, and Yury Gogotsi, Desolvation of ions in subnanometer pores and its effect on capacitance and double-layer theory, Angew. Chem. **120**, 3440 (2008).

[8] John R. Miller, R. A. Outlaw, and B. C. Holloway, Graphene double-layer capacitor with ac line-filtering performance, Science **329**, 1637 (2010).

[9] Martin Z. Bazant, Katsuyo Thornton, and Armand Ajdari, Diffuse-charge dynamics in electrochemical systems, Phys. Rev. E **70**, 021506 (2004).

[10] V. Novotny and M. A. Hopper, Optical and electrical characterization of electrophoretic displays, J. Electrochem. Soc. **126**, 2211 (1979).

[11] V. Novotny, Electrical conduction in surfactant-water-nonaqueous liquid systems, J. Electrochem. Soc. **133**, 1629 (1986).

[12] V. Novotny and M. A. Hopper, Transient conduction of weakly dissociating species in dielectric fluids, J. Electrochem. Soc. **126**, 925 (1979).

[13] Pavel Kornilovitch and Yoocharn Jeon, Transient electrophoretic current in a nonpolar solvent, J. Appl. Phys. **109**, 064509 (2011).

[14] Ming F. Hsu, Eric R. Dufresne, and David A. Weitz, Charge stabilization in nonpolar solvents, Langmuir **21**, 4881 (2005).

[15] Adrian Klinkenberg and Johan Leonard van der Minne, *Electrostatics in the Petroleum Industry: The Prevention of Explosion Hazards* (Elsevier, New York, 1958).

[16] Ian D. Morrison, Electrical charges in nonaqueous media, Colloids Surf. A **71**, 1 (1993).

[17] Tom Bert, Herbert De Smet, Filip Beunis, and Kristiaan Neyts, Complete electrical and optical simulation of electronic paper, Displays **27**, 50 (2006).

[18] Qiong Guo, Virendra Singh, and Sven Holger Behrens, Electric charging in nonpolar liquids because of nonionizable surfactants, Langmuir **26**, 3203 (2010).

[19] A. D. Hollingsworth and D. A. Saville, A broad frequency range dielectric spectrometer for colloidal suspensions: Cell design, calibration, and validation, J. Colloid Interface Sci. **257**, 65 (2003).

[20] Benjamin A. Yezer, Aditya S. Khair, Paul J. Sides, and Dennis C. Prieve, Use of electrochemical impedance spectroscopy to determine double-layer capacitance in doped nonpolar liquids, J. Colloid Interface Sci. **449**, 2 (2015).

[21] Filip Strubbe, Alwin R. M. Verschueren, Luc J. M. Schlangen, Filip Beunis, and Kristiaan Neyts, Generation current of charged micelles in nonaqueous liquids: Measurements and simulations, J. Colloid Interface Sci. **300**, 396 (2006).

[22] Filip Beunis, Filip Strubbe, Matthias Marescaux, Jeroen Beeckman, Kristiaan Neyts, and Alwin R. M. Verschueren, Dynamics of charge transport in planar devices, Phys. Rev. E **78**, 011502 (2008).

[23] Martin Z. Bazant, Kevin T. Chu, and B. J. Bayly, Current-voltage relations for electrochemical thin films, SIAM J Appl. Math. **65**, 1463 (2005).

[24] Peter Debye and Hans Falkenhagen, Dispersion of the conductivity and dielectric constants of strong electrolytes, Phys. Z. **29**, 121 (1928).

[25] Joseph Abate and Ward Whitt, A unified framework for numerically inverting Laplace transforms, INFORMS Journal on Computing **18**, 408 (2006).

[26] James Ross Macdonald, Theory of the differential capacitance of the double layer in unadsorbed electrolytes, J. Chem. Phys. **22**, 1857 (1954).

[27] M. V. Dyke, *Perturbation Methods in Fluid Mechanics* (Parabolic Press, Stanford, California, USA, 1975).

[28] M. Gouy, Sur la constitution de la charge électrique à la surface d'un électrolyte, J. Phys. Theor. Appl. **9**, 457 (1910).

[29] David Leonard Chapman, Li. A contribution to the theory of electrocapillarity, Philos. Mag. Ser. 6 **25**, 475 (1913).

[30] Mustafa Sabri Kilic, Martin Z. Bazant, and Armand Ajdari, Steric effects in the dynamics of electrolytes at large applied voltages. I. Double-layer charging, Phys. Rev. E **75**, 021502 (2007).

[31] Mustafa Sabri Kilic, Martin Z. Bazant, and Armand Ajdari, Steric effects in the dynamics of electrolytes at large applied voltages. II. Modified Poisson-Nernst-Planck equations, Phys. Rev. E **75**, 021503 (2007).

[32] J. J. Bikerman, XXXIX. Structure and capacity of electrical double layer, Philos. Mag. Ser. 7 **33**, 384 (1942).

[33] D. Gillespie, A review of steric interactions of ions: Why some theories succeed and others fail to account for ion size, Microfluid. Nanofluid. **18**, 717 (2015).